Tanzania Journal of Engineering and Technology 2022, **41(4)**:229-246
OPEN ACCESS articles distributed under Creative Commons Attribution Licence [CC BY-ND]
Websites: https://www.ajol.info/index.php/tjet; https://tjet.udsm.ac.tz


ISSN 1821-536X (**print**); ISSN 2619-8789 (**electronic**)
DOI: https://doi.org/10.52339/tjet.v41i4.863

*Full Length Review Paper*

# Review of the Imaging Performance and the Current Status of the Cascade Gamma-Rays Coincidence Imagers

**Leonid L. Nkuba[1*], Innocent J. Junior[2], Salum M. Mohamed[3], Innocent J. Lugendo[1], Najat K. Mohammed[4]**

[1]*Department of Physics, University of Dar es Salaam, P.O. Box 35063, Dar es Salaam, Tanzania.*

[2]*Dar es Salaam University College of Education, P.O. Box 2329, Dar es Salaam, Tanzania.*

[3]*Directorate of Technology and Technical Services, Tanzania Atomic Energy Commission, P.O. Box 743, Arusha, Tanzania.*

[4]*Dar es Salaam Institute of Technology, Bibititi and Morogoro Rd Junction, P.O. Box 2958, Dar es Salaam, Tanzania.*

[*]Corresponding email: *leonid_nkuba@yahoo.co.uk*; ORCID: https://orcid.org/0000-0002-5722-6380

## ABSTRACT

**Various studies that have investigated the detection of gamma coincidence events have revealed that design factors and image reconstruction approaches dictate the spatial resolution, coincidence efficiency, and levels of statistical noise of the detection system. In the case of imaging, cascade gamma-ray coincidence (CGC) imagers coupled with collimated detectors offer promising values for both spatial resolution and coincidence efficiency. However, to date, no CGC imager with single or multiple collimated detectors has reported a performance level beyond 6.7 mm spatial resolution (FWHM) and 6.0 × $10^{-6}$ coincidence efficiency. Given the recent developments and the current interests in high resolution and localization of an individual decaying nucleus, there is a need for CGC imagers with higher performance in terms of spatial resolution and efficiency. Therefore, deploying a CGC imager coupled with multiple collimated detectors may prove to be of value in nuclear imaging and probably in clinical applications**

ARTICLE INFO

Submitted: **October 28, 2022**

Revised: **December 11, 2022**

Accepted: **December 18, 2022**

Published: **December 30, 2022**

**Keywords:** *Cascade gamma-rays, Coincidence imager, Spatial resolution, Coincidence efficiency, and Signal to Noise ratio*.

## INTRODUCTION

Considerable progress has been reported in the emission computed tomography for three-dimensional (3D) imaging of radioactive point sources and/or radiopharmaceuticals in nuclear medicine and clinical research. According to Rahmim and Zaidi (2008), two major approaches, namely Single photon computed tomography (SPECT) and Positron emission tomography (PET) have been effectively used. SPECT is based on single photon counting while PET is based on coincident detection of annihilation gamma rays from the positron-emitting radionuclides. Although both approaches rely heavily on computerized image reconstructions, the physical collimation feature gives SPECT scanner an edge over the PET scanner in terms of image resolution, but at the expense of sensitivity. The photon-limited schemes, that is, physical collimation for SPECT and electronic collimation for PET always

maintain a tradeoff between resolution and sensitivity (Cherry *et al.,* 2012). However, the present-day nuclear medicine diagnostic tools i.e., SPECT and PET lack information on the emission points of individual decay nuclei, instead, they resort to statistical backprojection methods for image reconstructions (Rangacharyulu *et al.,* 2018). Several studies identify the issue, and many solutions are proposed and are being experimented (Saffer *et al.,* 1992; Shimazoe *et al.,* 2017; Rangacharyulu *et al.,* 2018; Santosh *et al.,* 2019). However, when there is a need for the precise location of an individual decaying nucleus, a different imaging approach is required.

One of the important imaging approaches is the one based on cascade gamma-ray coincidence imaging (Spyrou *et al.,* 2000; Shimazoe *et al.,* 2017; Rangacharyulu *et al.,* 2018; Santosh *et al.,* 2019; Panaino *et al.,* 2020; Rangacharyulu *et al.,* 2020). Cascade gamma-ray coincidence (CGC) imaging is referred to as the instance whereby two gamma-ray photons from a single decay are detected in coincidence with a pair of detectors (Saffer *et al.,* 1992). As these gamma-ray cascades are emitted at the location where the nucleus is decaying, thus, event-by-event analysis determines the decay vertices of stationary nuclei, and also the emissions are devoid of blurring from random positron motions (Rangacharyulu *et al.,* 2018; Panaino *et al.,* 2020). These cascade gamma rays can potentially be detected in coincidence and may be used to create images based on the gamma-gamma coincidence imaging concept (Pahlka *et al.,* 2018). Since the early 1960s, several researchers attempted to design imagers that measure the distribution of radioisotopes which emits gamma ray photons in cascade. These researchers pointed out that coincidence imaging of the cascade gamma rays with collimated detectors could be the future of nuclear medical imaging (Monahan and Powell, 1973; Boetticher *et al.,* 1979; Boetticher *et al.,* 1982). This article aimed at reviewing the CGC imagers based on design factors (geometrical design), image point reconstruction methodology, and imaging performances in terms of coincidence efficiency, spatial resolution in terms of full width at half maximum (FWHM), and signal-to-noise ratio (SNR).

This review aims to summarise the CGC imager's performance and document the CGC imager design with higher coincidence efficiency, acceptable levels of spatial resolution (FWHM), and a higher SNR. This review is important because the CGC imagers are capable of locating the position of an individual decaying nucleus. This is not possible for conventional PET and SPECT imaging systems. Apart from the imaging performances mentioned in this article, the description of possible clinical applications of the CGC imagers was also presented. Since the articles reporting on the CGC imagers developed from the 1960s to 1980s have been already reviewed by Chung *et al.* (1980), the current review presents the CGC imagers developed from the 1980s to early 2022.

## THE REVIEW OF CASCADE GAMMA-RAYS COINCIDENCE IMAGERS

### Earlier works in CGC imaging

A review by Chung *et al.* (1980) highlighted the breakthrough in the development of CGC imagers. One of the earlier CGC imagers called the *linear scanner* was capable of imaging five-point sources 2 mm apart and was capable of scanning and detecting cold spots within hot environments. However, the CGC imager was severely limited by random coincidences and low efficiency (Schmitz-Feuerhake, 1970). Helmers *et al.,* (1979a and 1979b) improved the efficiency of a linear scanner by replacing the scanner head with a collimated scintillator detector.

Random rate and low efficiency in scintigraphy were investigated by von Boetticher *et al.,* (1979). In their study, the optimal time resolution (τ) between coincidence was estimated for random event minimization. Also, the larger NaI(Tl) detectors replaced the smaller ones for efficiency improvement. However, due long light pulse of the NaI(Tl), the time resolution (τ) was deteriorated while maintaining the same level of efficiency loss as reported by Schmitz-Feuerhake (1970). Another CGC imager called *Total Organ Kinetic Imaging Monitor (TOKIM)* was developed. The TOKIM successfully visualized hot cylinders with diameters greater than 3.8 cm. However, TOKIM was limited by a very low geometrical efficiency (Powell and Monahan, 1970; Monahan and Powell, 1973) as it consists of only two gamma cameras aligned at 90 degrees. Two versions (FCCSI and FCCSII) were designed for another scanner called *Focused Collimator Coincidence Scanner (FCCS)*. The FCCSI was capable of clearly detecting cold spots (Hart, 1965). The efficiency of FCCSII was better than that of FCCSI since it uses five probes instead of two (Zacuto *et al.,* 1976; Hart and Rudin, 1977). Moreover, FCCSII was able to resolve two-point sources which are 5 mm apart. FCCSII reported also a FWHM of 6-7 mm in transverse and 12 mm in the longitudinal direction and a cold sphere greater than 7.5 mm was visible (Hart and Rudin, 1977). As in FCCSI, the FCCSII suffered from higher rates of random coincidences.

Some of the earlier CGC imagers based on multiple collimated detectors (Helmers *et al.*, 1982), time-of-flight (Powell, 1989), and collimatorless (Saffer *et al.,* 1992) were published after the review by Chung *et al.* (1980). These CGC imagers are discussed in this article. The review is based on their geometrical design, and performance in terms of coincidence efficiency and FWHM (mm). The factors that limit their performances are also presented.

***CGC imager with multiple collimated detectors surrounding a source***

According to Helmers *et al.,* (1979a), the first prototype scanner aimed to improve efficiency was designed. In 1982, this group of researchers added more detectors as shown in Figure 1, aiming at acquiring more coincidence events (Helmers *et al.,* 1982). Through the use of a liver phantom filled with $^{75}$Se, the cold spots in a stratified layer within a region of higher activity were not visible in the normal scanning (single photon counting). However, through the use of cascade gamma-ray coincidence imaging the cold spots were visible. Despite improved efficiency, this prototype scanner suffered from higher rates of random coincidence events.

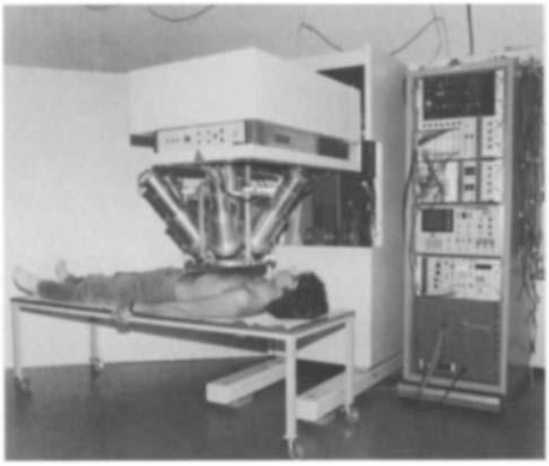

**Figure 1: 3D-scanner with multiple detectors (Helmers *et al.*, 1982).**

In 1982, another group of researchers designed a scintigraphic system that consists of a gamma camera and additional two detectors coupled with focusing slit collimators. The two detectors were aligned at 180 degrees Through measuring γ-γ coincidences, this imager was able to image scanned objects (von Boetticher *et al.*, 1982). The analysis of reconstructed images shows that the phantom studies had contrast enhancement through imaging of hot and cold spots in lengthy objects. They concluded that, through the use of pinhole collimators, the system sensitivity can be increased significantly.

***CGC imager based on time-of-flight information: a combination between the collimated detector and uncollimated detector***

In 1989, a coincidence imaging method which rely on the difference in time-of-flight (TOF) between the cascade gamma-ray photons originating from a single decay was proposed (Powell, 1989). Based on the geometry given in Figure 2, usually, a coincidence event is formed by acquiring information from cascade emitted gamma-ray photons from the same decay. The first gamma-ray is detected at $F_0$ (collimated detector) and the second gamma-ray is detected at $F_n$ (uncollimated detector). By applying a short coincidence time resolution (τ) window, the TOF difference between the two photons emitted in cascade can be estimated. The difference in path lengths of the two gamma rays emitted in cascade can be determined using the estimated TOF. The hyperboloid ($H_n$ ) surface is established using the path length difference ($F_0$) and the location of the foci ($F_n$). Finally, a point of intersection between the established hyperboloid surface and the line created by a gamma ray in a collimated detector gives the decay vertex of the nucleus (Liang and Jaszczak, 1990).

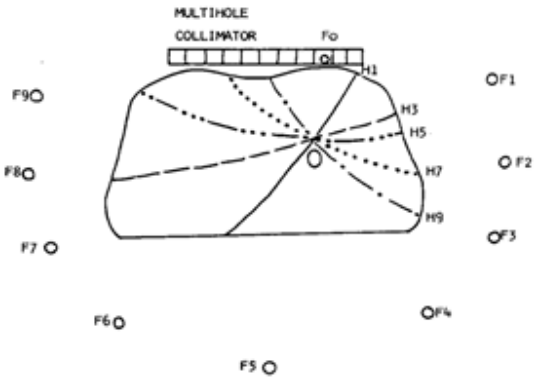


**Figure 2: Time of flight geometry (Powell, 1989).**

No prototype imaging experiments were performed; however, it was reported that the coincidence detection efficiency of the proposed CGC-based TOF imager could approach 50% of that of collimated detectors. However, this will depend on the type of radionuclide used (Powell, 1989). The limitation of the proposed method was the availability of detectors with sufficiently fast coincidence resolving time.

***CGC Collimatorless imager: Collimatorless, and without TOF information***

In the early 1990s, a group of researchers designed a CGC imager that does not use collimators or TOF information for image reconstruction as shown in Figure 3 (Saffer *et al.,* 1992). In their study, an array of 100 uncollimated planar detectors was used to view the scanned object in 3D. Through neglecting physical processes (i.e., attenuation and scatter, which may lead to a loss or change direction of a photon) encountered by a photon traversing in a material. An isotropically emitted single photon from point *R* is having a probability of being detected at *i*. The said probability is related to the solid-angle ΔΩ subtended by detector *i.*

$$P(1\ gamma\ ray) = \frac{1}{4\pi}\Lambda\Omega = \frac{\varepsilon^2 \cos^3\theta_1(R)}{z^2} \quad (1)$$

where $\varepsilon^2$ is the detector surface area, $\theta_i(R)$ is the angle between the normal to the *i*th detector and location ***R,*** and z is the vertical distance from *R* to the detector plane. The detector efficiency is assumed to be unity.

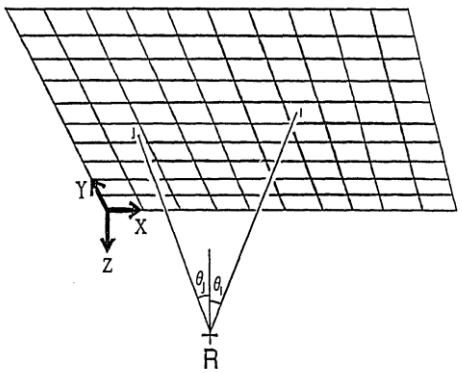


**Figure 3: Geometry of the detection system (Saffer *et al.*, 1992).**

Coincidence imaging requires two cascade gamma rays from the same decay to reach a set of detectors. Usually, these cascade gamma rays are emitted isotropically and independently. Thus, the probability of coincidence is proportional to the product of the solid angles subtended by detectors *i* and *j* as given in Equation (2).

$$P(2\ photons) = \frac{\varepsilon^4}{16\pi^2}\frac{\cos^3\theta_i(R)}{z^2}\frac{\cos^3\theta_i(R)}{z^2} \quad (2)$$

Through the use of pseudoinverse derived from the singular value decomposition (SVD), it was possible to reconstruct the source emission positions (Saffer *et al.* 1992). Figure 3, illustrates how the reconstructed image points do not depend on collimators or time-of-flight information (Saffer *et al.,* 1992). This method favored the sources near the detectors as distant sources (along the -z direction) are characterized by having a low probability of contributing to the acquired data, hence making them not visible to the detectors. The imager suffered from a rapid falloff in sensitivity for sources which are far from a detector plane. The term $1/z^4$ in Equation (2) is the reason for the rapid decrease in system sensitivity. Apart from sensitivity loss and invisibility of distant sources, this imaging modality offers higher resolution to sources near the detectors and is characterized by having a higher signal-to-background ratio (Saffer *et al.,* 1992). Besides the earlier prototypes, the latest CGC prototype imagers were also discussed.

## Recent works in CGC imaging

Recently, due to advancements in science and technology, several research groups modified earlier ideas by attaching highly sensitive electronic logic to gamma cameras with parallel hole collimators (Shimazoe *et al.*, 2017; Pahlka *et al.*, 2018; Uenomachi *et al.,* 2021). To improve coincidence efficiency and spatial resolution, one of the groups used a single gamma camera coupled with focused collimators (Choghadi *et al.,* 2021), while the other group designed a CGC imager with dual gamma cameras; one of the cameras equipped with multi-slit collimator and other with multi-pinhole (Lui *et al.,* 2021). The use of Compton scattering kinetics emerged as another mode of CGC imaging. A group of Yoshihara *et al.* (2017) and Uenomachi *et al.* (2018), used Compton cameras to carry out CGC imaging. While other groups used Compton PET hybrid detectors to realize the CGC imaging (Omata *et al.,* 2020; Omata *et al.,* 2022). Finally, another group of researchers employed TOF information to determine the location of source emission via simulation (Chiang *et al.,* 2020). A detailed review based on coincidence efficiency, spatial resolution, and possible clinical application is given in the article.

### *CGC imager with dual gamma cameras coupled with parallel holes collimators*

Several researchers embarked on creating coincidence-based images from cascade gamma photons. Pahlka *et al.* (2018) designed the CGC imager through simulations (Geant4). The imager consisted of two collimated (parallel holes) gamma cameras oriented at the right angle. From their study, coincidence-based images were created by finding the mild point coordinate of two skew lines created from collimator projections (normal vector in red) as illustrated in Figure 4. In their study, $^{111}$In isotope with 171.3 keV and 245.4 keV cascade photons and 85 ns half-life of the intermediate state was used.

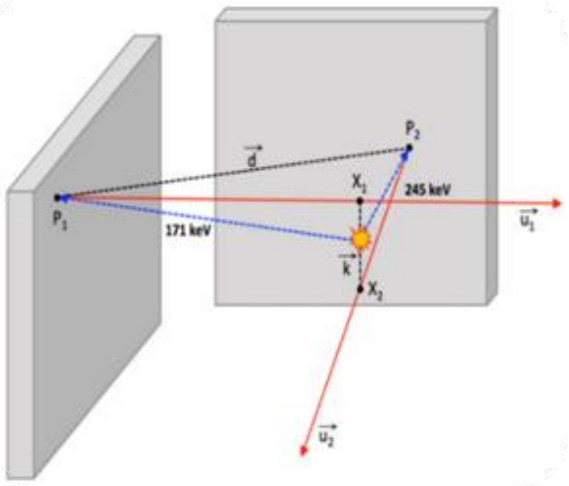


**Figure 4: Illustration of the image reconstruction procedure (Pahlka *et al.*, 2018).**

Results show that the coincidence efficiency for a single point source in air, at the center of the field of view, was $6.0 \times 10^{-8}$ and the computed FWHM resolutions were 8.0 mm and 12.1 mm for the axial and transverse directions, respectively. Further in their analysis, they concluded that images reconstructed with larger time coincidence windows are having poor resolution due to the inclusion of random coincidence events during image reconstruction. According to Pahlka *et al.* (2018), the imager geometry, reconstruction method and acquired coincidence events from cascade gamma rays are not sufficient for the production of diagnostic images. Thus, coincidence imaging via cascade gamma rays alone is not clinically viable. However, information from cascade gamma-ray coincidence imaging can be used as an addition to information (events) acquired in SPECT imaging.

Another research group proposed a coincidence imaging method called double photon emission computed tomography (DPECT). In the DPECT method, dual detectors aligned at 90 degrees were used. As shown in Figure 5, the designed CGC imager consists of two mechanically collimated (parallel holes) detectors. The source position, which is a 3D point, is then determined through the calculated point of intersection between two collimator projections stemming from true coincidence events (Shimazoe *et al.*, 2017).

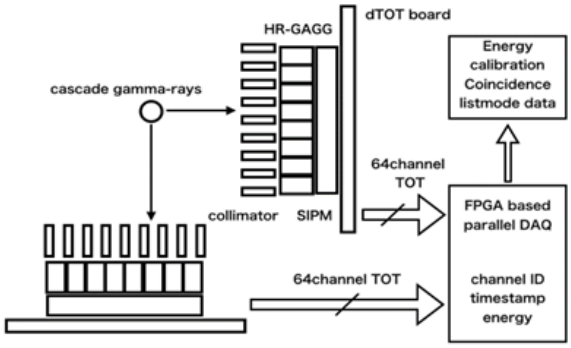


**Figure 5: The experimental setup ( Shimazoe *et al.*, 2017).**

The measured FWHM resolution of a syringe containing $^{111}$In (171.3 keV and 245.4 keV) source is ~4.08 mm. The measured FWHM value resembles the actual size of the syringes' diameter. Analysis of reconstructed images shows that the coincidence-based images were good, with no background. The DPECT (CGC-imager) imager successfully visualized in 3D the $^{111}$In source contained in a syringe with stationary detectors. No any sophisticated image reconstruction algorithms were used. Reconstructed image without coincidence (single photon) between the cameras was affected by the source background. Hence, coincidence

imaging offers a higher signal-to-background ratio compared to single photon imaging.

In their later research, this group proposed another crosstalk reduction method. In their study, simultaneous imaging of two sources possessing cascade decay was possible via the DPECT method. Their CGC imager consisted of four GAGG detectors arranged at 90 degrees to each and equipped with parallel hole collimators as shown in Figure 6 (Uenomachi *et al.*, 2021a).

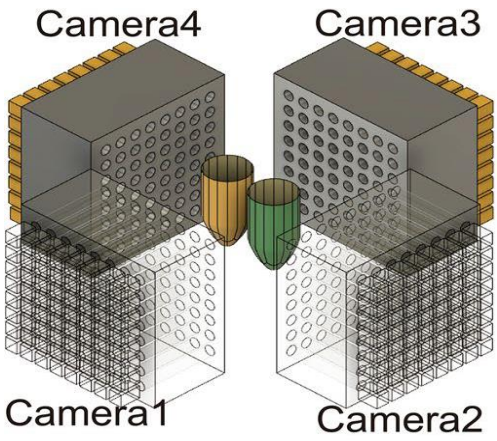


**Figure 6: Diagram of the experimental setup with $^{111}$In and $^{177}$Lu in microtubes (Uenomachi *et al.*, 2021a).**

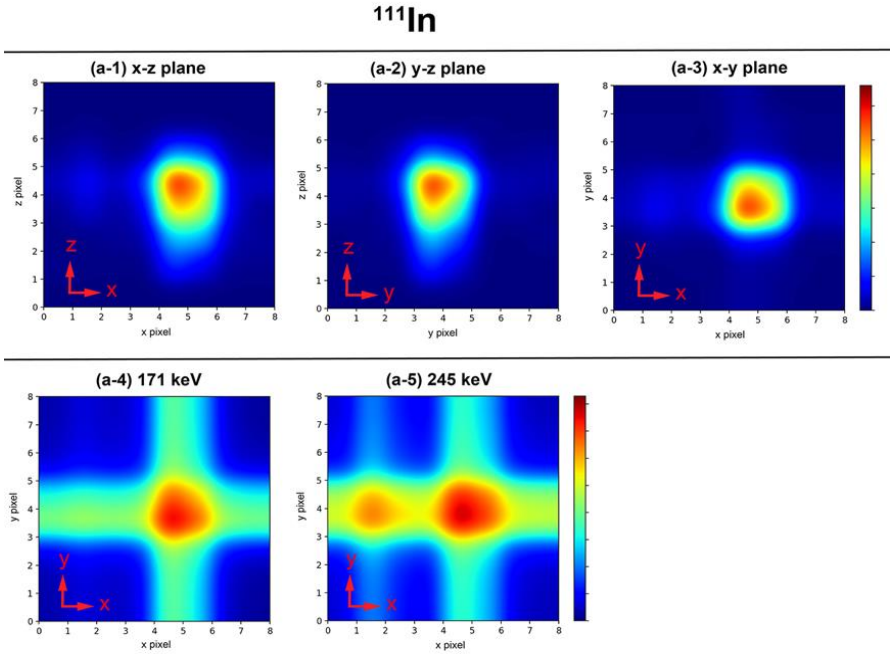


**Figure 7: Reconstructed images of $^{111}$In: (a-1 to a-3) 2D slice images of $^{111}$In by DPECT imaging. (a-4 & a-5) 2D slice images of $^{111}$In by 171 keV single-photon imaging, and 245 keV single-photon imaging in the *x–z* plane (Uenomachi *et al.*, 2021a).**

Results show that, for 3D imaging with DPECT (CGC-based method), the absolute coincidence efficiencies were $4.38 \times 10^{-8}$ and $2.51 \times 10^{-8}$ for $^{111}$In and $^{177}$Lu, respectively. As seen in Figure 7 (a-1 to a-3), the proposed CGC imaging method reduces the background resulting from the $^{177}$Lu source. The same phenomenon

occurred when the 3D images of the $^{177}$Lu source were reconstructed. This CGC imaging modality is having higher signal-to-noise ratio and offers images with better resolution compared to those acquired through conventional single photon imaging as illustrated in Figure 7 (a-4 & a-5) (Uenomachi *et al.*, 2021a). The limitation of this CGC imaging method is the low detection efficiency which is approximately $10^4$ lower than that of single-photon imaging.

***Cascade gamma coincidence imager with dual gamma cameras coupled with slit and pinhole collimators***

Recently, a group of researchers designed a CGC imager using two NaI(Tl) gamma cameras in the "L" shape as shown in Figure 8. Each of the gamma cameras was coupled with a different type of collimator (multi-slit and multi-pinhole). Because the gamma cameras were fixed, the CGC imager was named as a stationary cascade gamma-ray coincidence imager (SCGCI). $^{177}$Lu isotope was used in their study (Liu *et al.*, 2021). Their results were impressive. On the simulated imager, the coincidence efficiency at the center of the field of view was $3.85 \times 10^{-6}$, and the spatial resolution was 7.0 mm. On the prototype imager, the corresponding values were $3.20 \times 10^{-6}$ and 6.7 mm, respectively (Liu *et al.*, 2021). Figure 8(B) shows the reconstructed images and sectional profiles of five-point sources acquired from simulated SPECT and SCGCI imagers. For SPECT, images were reconstructed through filtered back-projection (FBP) of single emitted photons, while for SCGCI, images were reconstructed through double back projection (DBP) of cascade photons detected in coincidence. Despite low coincidence efficiency in the SCGCI compared to that of a conventional SPECT, the image resolution for SCGCI was much better than conventional SPECT (Figure 8B). Hence, this demonstrates that the 3D SCGCI is fully functional.

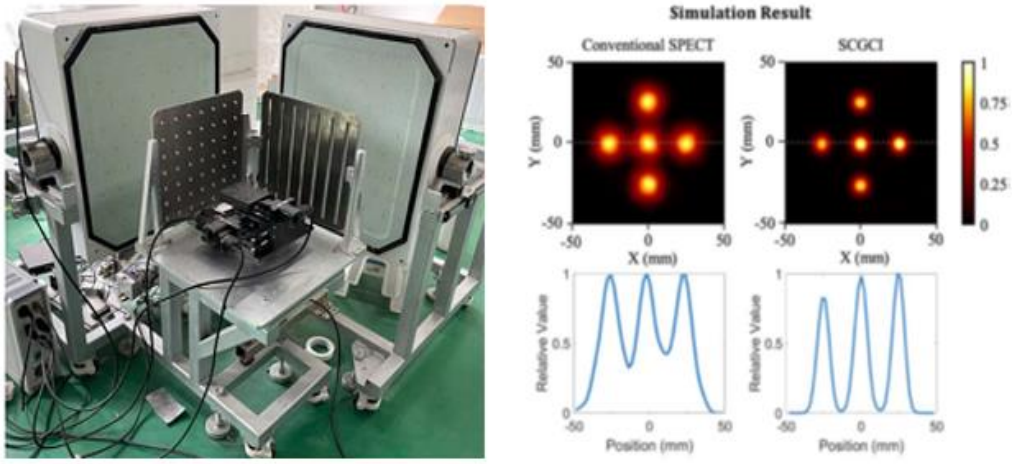


**Figure 8: (A) Picture of the imaging prototype, (B) Comparison of reconstructed five-point images using conventional SPECT and SCGCI (Liu *et al.*, 2021).**

***CGC imager with a detector coupled with a focused collimator***

Another group proposed a CGC imaging method which uses a single detector coupled with a focused collimator. This design aimed to improve detection efficiency. The single-detector CGC imaging model is described in Figure 9. In summary, for the CGC imaging model, only one detector is used to scan and detects information on one point (focal point) for a given time, and then moves to another point. The decaying

source information is acquired through a method called the step-and-scan procedure (Choghadi *et al.*, 2021). Unlike the conventional CGC method proposed by Shimazoe *et al.* (2017) and Pahlka *et al.* (2018), the proposed CGC imaging method does not have combination restrictions of detector pixels for coincidence detection. Thus, higher coincidence efficiency was obtained.

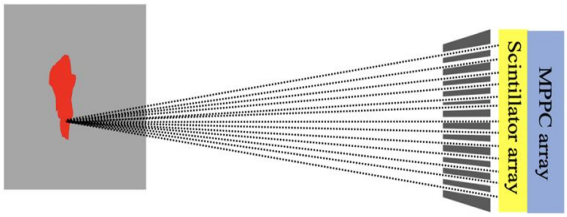


**Figure 9: The double-photon gamma scanner (Source: Choghadi *et al.*, 2021).**

In the prototype imaging experiment, a 1 MBq $^{111}$In (171.3 keV and 245.4 keV) solution in a microtube was scanned. A comparison of reconstructed images acquired through single-photon and double-photon (CGC) imaging of $^{111}$In solution is shown in Figure 10. The activity image with CGC corresponds to the scanned source more closely with no background activity (Figure 10B). As can be seen in Figure 10(A), in the case of single-photon analysis, even outside the microtube there is a large background, while in the case of CGC imaging, there is no background and thereby the contrast is much better (Choghadi *et al.*, 2021).

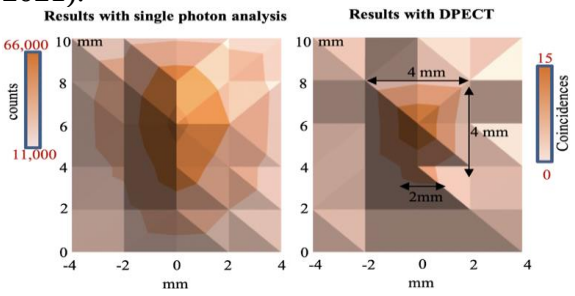


(A) (B)

**Figure 10: 2D Images-(A) Single photon analysis, (B) the new CGC method (Choghadi *et al.*, 2021).**

Despite the low coincidence efficiency which is approximately $1.6 \times 10^{-7}$, resulting from a small solid angle covered during the scanning, the signal-to-background ratio (SBR) of the single detector CGC imager is 5 times that of single-photon counting. Thus, the CGC imager provides better contrast images. The only issue in the single detector CGC imaging method was the step size of 2 mm which limits the spatial resolution.

### *CGC imager based on Compton scattering kinetics*

Several research groups proposed a novel method of image reconstruction based on coincidence detection for cascade gamma-rays with multiple Compton cameras (Yoshihara *et al.*, 2017; Uenomachi *et al.*, 2018). This method is based on Compton kinetics. Unlike conventional Compton imaging, which uses a single Compton event (from a single photon) and reconstructs one Compton cone on the projection plane as in Figure 11(a), in the double-photon (CGC) Compton imaging, coincidence events are extracted from both detectors (Detector 1 and Detector 2). The image point is obtained by drawing intersections of two Compton cones as shown in Figure 11(b). Each Compton cone is defined by the scattering angle and the cone axis constructed from the two hit positions of the gamma-ray (Yoshihara *et al.*, 2017).

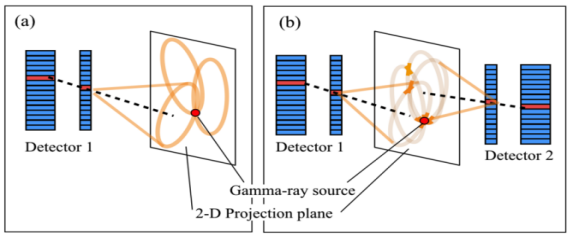


**Figure 11: (a) Single Compton imaging and (b) Double coincidence Compton imaging ( Yoshihara *et al.*, 2017).**

Figure 12 shows the 2D images from conventional (single-photon) Compton and double-photon (CGC) Compton imaging. Results show that the CGC Compton imaging method has a coincidence efficiency of $3.56 \times 10^{-6}$, $5.67 \times 10^{-6}$, and

$3.09 \times 10^{-6}$, signal to noise ratio of 35.97, 29.59 and 32.57 as well as spatial resolution ranging from 28.13-29.87 mm, 31.92-34.18 mm and 26.61-36.30 mm for $^{111}$In, $^{134}$Cs and $^{60}$Co, respectively.

The analysis of results using simulation and prototype imaging data indicated that, though its detection efficiency is much lower than that of the single photon Compton imaging method by a factor of $10^3$, the CGC Compton imaging method is having better spatial resolution and 4.5 – 5.4 times higher SNR than single Compton imaging method for each nuclide under the study (Yoshihara *et al.*, 2017).

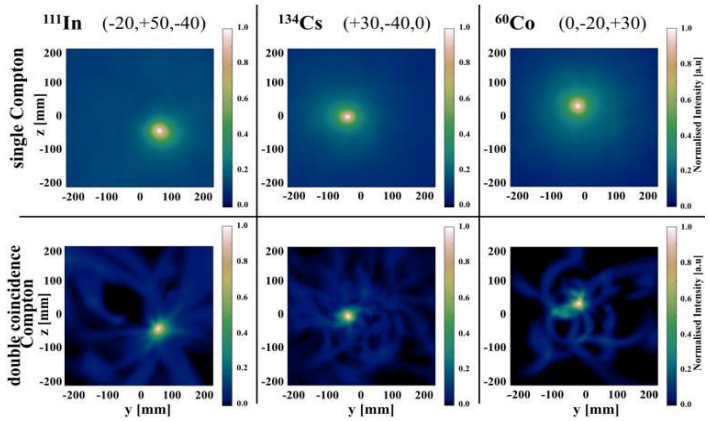


**Figure 12: The 2D map images using single Compton events and double coincidence Compton events (Yoshihara *et al.*, 2017).**

The CGC Compton imaging method can be applied in the area where high-contrast images are needed. Also, the method is suitable for imaging where there is much background radiation. For instance, it has been observed that high contrast was achieved between the target nuclide of $^{134}$Cs or $^{60}$Co under the major background nuclide of $^{137}$Cs (Yoshihara *et al.*, 2017; Uenomachi *et al.*, 2018). Moreover, it could visualize distributed $^{111}$In-DTPA in the body, which would contribute to real-time monitoring of the neuron network (Yoshihara *et al.*, 2017).

Another group of researchers designed a CGC imager with a Compton-PET hybrid camera (Uenomachi *et al.*, 2021b). Their research aimed at combining PET (with $^{18}$F) and SPECT (with a $^{111}$In) imaging. Combining PET and SPECT into a single imaging system was difficult as SPECT requires physical collimators. Therefore, a novel imaging method that can image SPECT and PET nuclides in a single scan was designed by combining PET (with $^{18}$F) and Compton (with a $^{111}$In) imaging systems as illustrated in Figure 13. Usually, Compton imaging does not require physical collimators, it has a forward layer called scatter and a second layer called absorber (detector). This method has been proven of being capable of visualizing gamma rays over a wide range of energies.

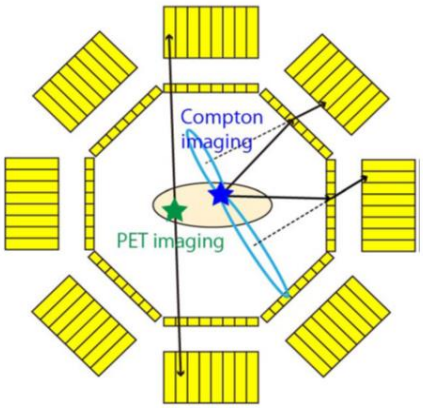


**Figure 13: The Compton-PET hybrid camera (Uenomachi *et al.*, 2021b).**

In their study, the spatial resolution by measuring the $^{22}$Na and $^{18}$F point sources was performed to evaluate the performances between the two (PET and Compton) imaging models. Figure 14(a) shows the reconstructed image of $^{22}$Na by using the

Backprojection (BP) method in PET imaging. For PET imaging, the spatial resolution was 3.3 mm FWHM and 3.3 mm FWHM along the horizontal and vertical axes, respectively. For Compton imaging at 511 keV, the spatial resolution values were slightly poor as shown in the reconstructed image of $^{18}$F given in Figure 14(b). Reported spatial resolution values for a point source image in Figure 14(b) were 4.2 mm FWHM and 3.8 mm FWHM along the horizontal and vertical axes, respectively The Compton image was reconstructed by using the maximum-likelihood expectation–maximization (MLEM) method after 60 iterations (Uenomachi *et al.*, 2021).

Further in their research, a simultaneous in vivo imaging of a tumor-bearing mouse injected with $^{18}$F-FDG and $^{111}$In ($^{111}$In-antibody) by using a prototype Compton-PET hybrid camera was demonstrated. The results indicated that the visualization of accumulations of $^{18}$F-FDG and $^{111}$In-antibody by performing PET imaging and Compton imaging simultaneously was successful. As simultaneous imaging utilizes the same coordinate axes, it is expected to improve the accuracy of diagnoses (Uenomachi *et al.*, 2021b). Another group of researchers developed a "hybrid" Compton camera that can image x-rays and gamma rays at the same time by combining desired features of "Compton" and "pinhole" cameras in a single detector system (Omata *et al.*, 2020). Similar to conventional CGC Compton cameras reported by (Uenomachi *et al.*, 2018), the Compton hybrid camera consists of two layers of scintillator arrays.

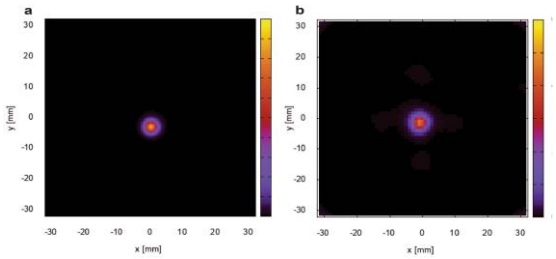


**Figure 14: Imaging results. (a) PET image of $^{22}$Na point source, (b) Compton image of $^{18}$F point source. (Uenomachi *et al.*, 2021b).**

The forward layer usually acts as a scatterer for high-energy photons (> 200 keV) and an active pinhole for low-energy photons (< 200 keV) as shown in Figure 15. The other layer acts as a detector, where the gamma radiation deposits most of its energy to create pulses.

Results showed that simultaneously acquired images of $^{241}$Am (60 keV) and $^{137}$Cs (662 keV) point sources, achieved an angular resolution (FWHM) of $10^0$ for each of the two scanned sources. To demonstrate the system's viability, The "L"-shaped $^{241}$Am extended source was scanned. Its images were reconstructed by the pinhole mode using events with energies around 60 keV.

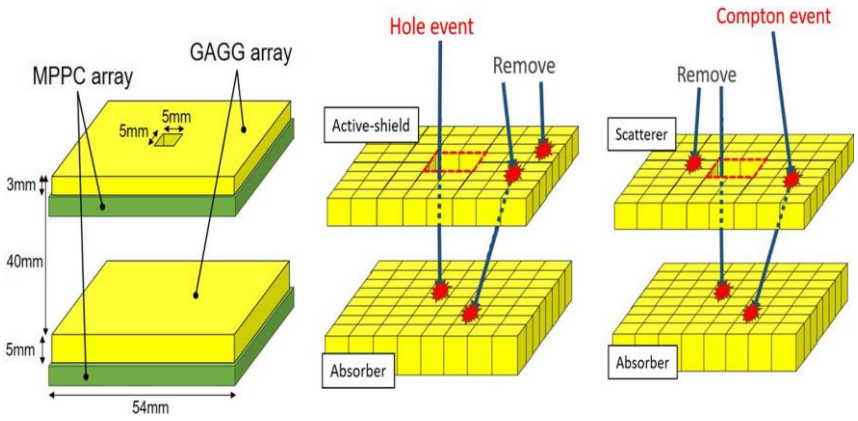


**Figure 15: The hybrid camera (*left*). The pinhole event mode (*center*) and the Compton event mode (*right*) (Omata *et al.*, 2020).**

To determine the difference between pinhole and Compton imaging mode, the images of an "L"-shaped $^{137}$Cs extended source (662 keV) were reconstructed by the Compton mode. In all the models, the MLEM algorithm was used for the reconstruction of L-shaped images as shown in Figure 16. In their study, they also observed that a mouse injected with 1.0 MBq of $^{211}$At can be scanned for one hour and imaged via pinhole mode (Omata *et al.*, 2020). By visualizing the reconstructed images, the images using pinhole mode had better resolution compared to their corresponding images acquired by Compton. Again, in their subsequent research paper, they developed a hybrid Compton camera (HCC) that contains three imaging modalities in a single case: Compton, pinhole, and PET imaging (Omata *et al.*, 2022).

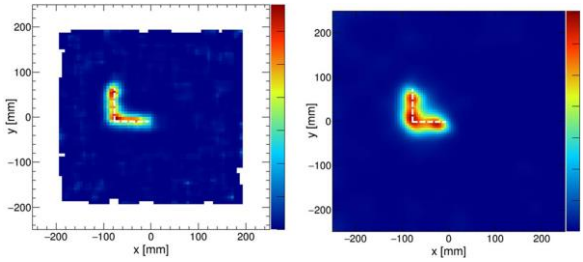


**Figure 16: The L-shaped reconstructed sources images via MLEM. Pinhole reconstruction of the $^{241}$Am source (*left*) and Compton reconstruction of the $^{137}$Cs source (*right*) ( Omata *et al.*, 2020).**

The developed system consists of four HCCs to extend pinhole/Compton imaging to 3D space as illustrated in Figure 17. Three sources: $^{137}$Cs (904 kBq), $^{22}$Na (45 kBq), and $^{241}$Am (3.93 MBq) were used to test the imaging performance of the multi-modal 3D imager. All three sources were scanned simultaneously.

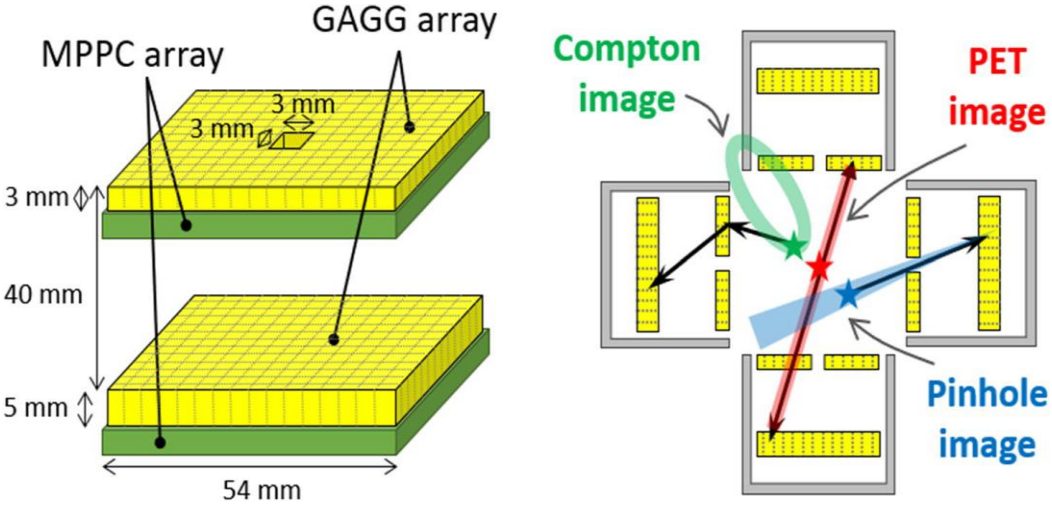


**Figure 17: The hybrid Compton camera (*Left*). Schematic of reconstruction in multi-modality (*right*): Compton, PET, and pinhole imaging (Omata *et al.*, 2022).**

Results showed that simultaneous imaging of $^{137}$Cs (Compton mode targeting 662 keV), $^{22}$Na (PET mode targeting 511 keV), and $^{241}$Am (pinhole mode targeting 60 keV) within the same field of view was possible (Figure 18). Through the analysis of 1D projections of each source, which are coded as green, red, and blue conversions correspond to $^{137}$Cs (662 keV; Compton mode), $^{22}$Na (PET mode), and $^{241}$Am (60 keV; pinhole mode) sources, the Compton mode still suffer for poor resolution, followed by pinhole mode, while PET mode is reported to have good image resolution as its 1D projection is not broad (Omata *et al.*, 2022). In addition, the imaging of $^{67}$Ga and

$^{111}$In, which are used in various diagnostic scenarios was conducted. In their study, they verified that the 3D distribution of the $^{211}$At tracer inside a mouse could be imaged using the pinhole mode.

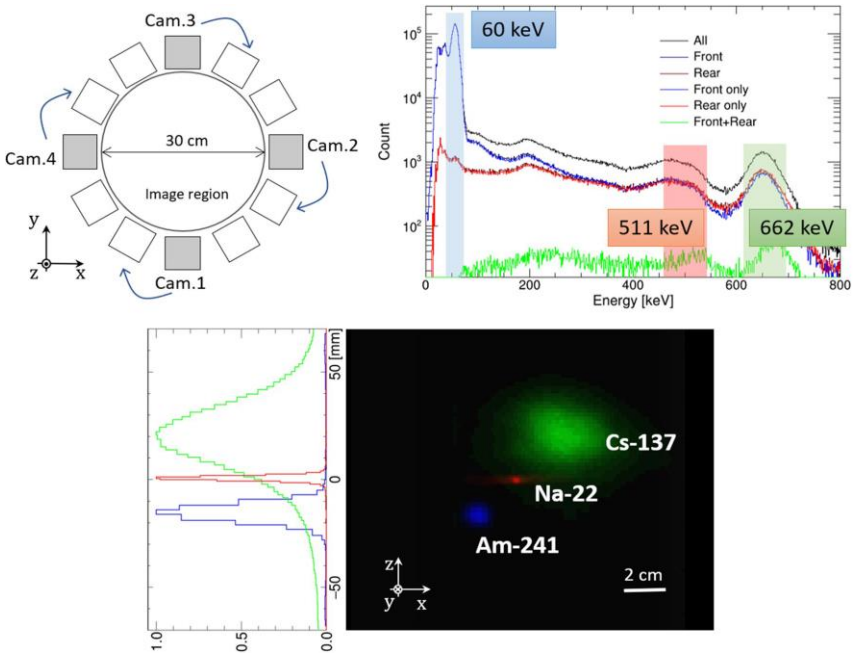


**Figure 18: Multi-angled measurement configuration (*Upper left*). Energy spectra for $^{137}$Cs, $^{22}$Na, and $^{241}$Am acquired via the HCC (*upper right*). The 3D reconstructed image (*lower right*) and their 1D projection profiles (*lower left*) (Omata *et al.*, 2022).**

### *CGC imager based on time-of-flight (TOF) information*

Recently, a group of researchers applied TOF information to image reconstruction, this group developed a method called the time-of-flight dual photon emission computed tomography (TOF-DuPECT). The TOF-DuPECT imaging method can obtain radionuclide distributions using time information recorded in coincidence from two cascade-decay photons. In their study, Monte Carlo simulations were used to realize the imager capabilities. The image reconstruction relies on the generated list-mode coincidence data. A full-ring PET detection system, with uncollimated detectors, was designed and modeled through simulation. In this feasibility study, the $^{75}$Se source was used in testing the viability of the imager. As shown in Figure 19, the source decay vertex can be determined using the estimated time-difference-of-arrival (TDOA) of the two cascade photons detected in coincidence and the global coordinates of the coincident detector pairs (Chiang *et al.*, 2020; Panaino *et al.*, 2020).

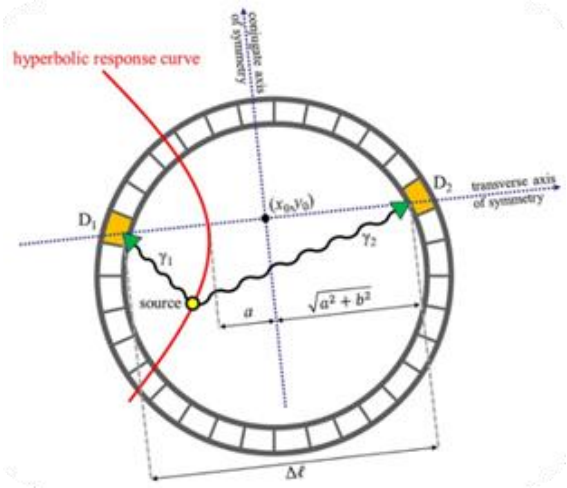


**Figure 19: Illustration of the TDOA technique (Source: Chiang *et al.*, 2020).**

Results show that the TOF-DuPECT imager is having a sensitivity of 0.4% (~4.0 × $10^{-3}$). However, after the application of the dual-energy window, the system sensitivity drops

to about ~ 0.2% (~2.0 × $10^{-3}$). As seen in Figure 20, the point source located in the central field of view progressively becomes blurrier whenever the CTR value increases (Chiang *et al.*, 2020).

The imaging result of the Jaszczak-like phantom with hot rods shows that the resolution gets better with decreasing CTR values. For instance, the smallest hot rods (15.4 mm) in the phantom were visible when an ideal CTR of 0 ps was applied. It has been observed that all hot roads were visible at a CTR of 50 ps. The smallest hot road (15.4 mm) remains barely visible until the CTR goes beyond 100 ps. The results show that the FWHM values at 1500 sweeps can reach ~20 mm when the CTR is less than 50 ps. For CTRs of 100 ps, 150 ps, and 200 ps, the measured FWHMs are 26.5 mm, 32.2 mm, and 40.1 mm, respectively. The findings of their study indicated that the TOF-DuPECT system employing the stochastic origin ensemble (SOE) algorithm, can yield quality images provided that the CTR less value is than 100 ps (Chiang *et al.*, 2020). The TOF-DuPECT imaging system offers higher sensitivity (no collimators) compared to conventional SPECT imaging systems with acceptable spatial resolution. However, the TOF-DuPECT system is primarily limited by the CTR values. For larger CTR values, reconstructed images with poor resolution are expected.

## The current status of CGC imagers

In this review, most of the earlier cascade gamma-ray coincidence imagers suffered from either low coincidence efficiency or poor spatial resolution or both low coincidence efficiency and poor spatial resolution. However, the CGC imaging methods offer higher SNR values and good FWHM resolution compared to conventional single photon imaging. Despite higher coincidence efficiency, the conventional (single photon) Compton imaging method specifically suffers from having poor spatial resolution and lower SNR compared to CGC Compton imaging methods. For the imaging method employing time of flight (TOF) information, despite good detector geometry which offered higher geometric acceptance and coincidence efficiency, the method is limited to the timing resolution of the detectors, poor spatial resolution for higher coincidence time resolution (CTR) and cost related issues for detectors with TOF capability. Apart from the TOF-DuPECT imager with a sensitivity of ~2.0 × $10^{-3}$ (Chiang *et al.*, 2020), Compton scattering kinetics CGC based-imager with a maximum coincidence efficiency of ~5.67 × $10^{-6}$ for $^{134}$Cs (Yoshihara *et al.*, 2017) and conventional CGC imager with coincidence efficiency of ~3.85 × $10^{-6}$ and ~3.20 × $10^{-6}$ (Liu *et al.*, 2021), so far, no other conventional CGC imager has reported a performance level beyond 6.0 × $10^{-6}$ coincidence efficiency. For spatial resolution (FWHM), the best results obtained ranged from 3.8 mm (vertical) to 4.2 mm (horizontal) from a Compton-PET hybrid camera with a 511 keV gamma-ray from $^{18}$F (Uenomachi *et al.*, 2021). However, this system is expected to inherit the limitations observed in conventional PET which include image blurring due to positron movement and the inability to locate the position of an individual decaying nucleus (Rangacharyulu *et al.*, 2018). For conventional CGC, the best spatial resolution was 6.7 mm (the prototype imager) to 7.0 mm (the simulated imager) from a cascade gamma coincidence imager equipped with dual gamma cameras, one of the cameras was equipped with multi-slit and the other with multi-pin hole collimators, with 208 keV and 113 keV gamma-rays from $^{177}$Lu (Liu *et al.*, 2021), respectively.

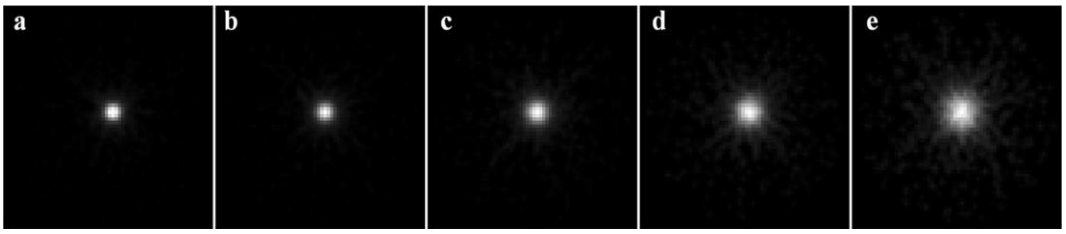


**Figure 20: Reconstructed point source images for different CTRs of (a) 0 ps, (b) 50 ps, (c) 100 ps, (d) 150 ps, and (e) 200 ps (Chiang *et al.*, 2020).**

## CONCLUSION AND RECOMMENDATIONS

This review paves the way for the development of a new CGC imager coupled with multiple collimated (parallel holes) detectors, which will offer a coincidence efficiency beyond $6.0\times10^{-6}$ and spatial resolution (FWHM) beyond 6.7 mm. With several detectors surrounding a source, the coincidence efficiency may be improved (Monahan and Powell, 1973). A large number of detectors is expected to rise the coincidence efficiency values above those of conventional CGC with dual gamma cameras reported in previous studies (Shimazoe *et al.*, 2017; Pahlka *et al.*, 2018). It is for this reason that, PET imaging assembly seems to be an appropriate set-up for developing a novel cascade gamma-ray coincidence-based imager because the detectors in PET are in a ring form (Santosh *et al.*, 2019; Rangacharyulu *et al.*, 2020), and hence the source will be surrounded by several detectors. However, for a CGC imaging modality to be implemented in the PET scanner, an additional retrofit of physical collimators is needed as in SPECT assembly (Santosh *et al.*, 2019; Rangacharyulu *et al.*, 2018; Rangacharyulu *et al.*, 2020). The introduction of physical collimators in the PET imaging system will require collimator optimization to acquire sufficient coincidence events and re-writing the image reconstruction algorithm to accommodate the cascade gamma-ray correlation emissions and physical changes in the PET assembly.

Based on the characteristics of cascade gamma-rays, which include the emission of cascade gamma rays at the location where the nucleus is decaying, and the emissions are devoid of blurring from random positron motions (Shimazoe *et al.*, 2017, Rangacharyulu *et al.*, 2018). Thus, the proposed CGC imager will be able to identify the location of an individual decaying nucleus, which is impossible in conventional PET and SPECT systems. A common concern regarding the proposed CGC imager is low coincidence efficiency. In the proposed CGC imager, the low coincidence efficiency will result from the loss of geometric efficiency due to physical collimation in the PET imaging system, the use of non-collinear coincidence events only in image reconstruction, and the physical nature of coincidence event detection. However, this loss will be overcompensated by the image reconstruction algorithm as each detected valid coincidence event, by itself, unambiguously locates the decay parent location and constitute an image point. On the other hand, random coincidence events will be minimized through the use of isotopes with shorter intermediate lifetime ($t$) between the cascade gamma-rays, and minimal coincidence time ($\tau$) resolution window of the system. In practice, the two parameters in the CGC imagers must obey the following inequality $t \leq \tau$ (Pahlka *et al.*, 2018). The CGC imager implemented in PET assembly coupled with optimized collimators is expected to offer good spatial resolution compared to conventional PET scanners.

## REFERENCES


Cherry S., Sorenson J. and Phelps M. (2012). Physics in Nuclear Medicine, 4th edn., 17&18: 279-322, Elsevier, Saunders., Philadelphia.

Chiang C.C., Chuang C.C., Ni Y.C., Jan M.L., Chuang K.S. and Lin H.H. (2020). Time of flight dual photon emission computed tomography, Scientific Reports, **10**(19514): 1-13.https://doi.org/10.1038/s41598-020-76526-z

Choghadi M.A., Kitajima M., Uenomachi M., Shimazoe K. and Takahashi H. (2021). Collimator-based Coincidence Imaging for Double Photon Emitting Nuclides. Radioisotopes, 70(4): 271–277.

Chung V., Chuen Chak Ki., Zacuto P. and Hart HE. (1980). Multiple Photon Coincidence Tomography. Seminars in Nuc Med, 10(4): 345-354.

Hart H.E. (1965) Focusing Collimator Coincidence Scanning. Radiology, 84: 126.

Hart H.E. and Rudin S. (1977). Three-Dimensional Imaging of Multimillimeter Sized Cold Lesions by Focusing Collimator Coincidence Scanning. IEEE Trans on Biom Eng, 24(2): 169-177.

Helmers H., Von Boetticher H. and Schmitz-Feuerhake I. (1979a) Scanner performance to overcome efficiency problems in three-dimensional scintigraphy by γ-γ-coincidences. Phys. Med. Biol., 24(5): 1025–1029.

Helmers H., von Boetticher H. and Schmitz-Feuerhake I. (1982). Depth-Discrimination in Direct 3D-Scanning Without Image Reconstruction Using A Coincidence Technique. Eur. J. Nucl. Med, 1: 324–326.

Helmers H., von Boetticher H., Schreiber P. and Schmitz-Feuerhake I. (1979b) Geometrical resolution and efficiency of two systems for three-dimensional scintigraphy by γ-γ-coincidences. XII Internal Conference on Medical and Biological Engineering and V International Conference on Medical Physics, Jerusalem, p 64.3

Liang Z. and Jaszczak R. (1990). Comparisons of Multiple Photon Coincidence Imaging Techniques. IEEE Trans on Nucl Sci, **31**(3): 1282-1292.

Liu X., Liu H., Cheng L., Wu J., Bao T., Yao R. and Liu Y. (2021). A 3-dimensional stationary cascade gamma-ray coincidence imager. Phys. Med. Biol, 66: 225001. 1-17. https://doi.org/10.1088/1361-6560/ac311b.

Monahan W.G. and Powell M.D. (1973). Three-dimensional imaging of radionuclide distribution by gamma-gamma coincidence detection. Tomographic Imaging in Nuclear Medicine, Society of Nuclear Medicine, Edited by Freedman OS for Society of Nuclear Medicine, New York, USA. pp 165-175.

Omata A, Masubuchi M, Koshikawa N, Kataoka J, Kato H, Toyoshima A., Teramoto T., Ooe K., Liu Y., Matsunaga K., Kamiya T., Watabe T., Shimosegawa E. and Hatazawa J. (2022). Multi-modal 3D imaging of radionuclides using multiple hybrid Compton cameras. Scientific Reports, **12**(2546): 1-9. https://doi.org/10.1038/s41598-022-06401-6.

Omata A., Kataoka J., Fujieda K., Sato S., Kuriyama E., Kato H., Toyoshima A., Takahiro Teramoto T., Ooe K., Liu Y., Matsunaga K., Kamiya T., Tadashi Watabe T., Shimosegawa E. and Hatazawa J. (2020). Performance demonstration of a hybrid Compton camera with an active pinhole for wide-band X-ray and gamma-ray imaging. Sci Rep, **10**(14064): 1-9. https://doi.org/10.1038/s41598-020-71019-5.

Pahlka R.B., Kappadath S.C. and Mawlaw O.R. (2018). A Monte Carlo simulation of coincidence detection and imaging of gamma-ray cascades with a scintillation camera. Biom. Phys. Eng. Expr, **4**(055012): 1-18. https://doi.org/10.1088/2057-1976/aad572.

Panaino C.M.V., Mackay R.I., Sotiropoulos M., Kirkby K.J. and Taylor M.J. (2020). Full 3D position reconstruction of a radioactive source based on a novel hyperbolic geometrical algorithm. Computer Physics Communications, 107131, https://doi.org/10.1016/j.cpc.2019.107131.

Powell M.D. (1989). Multiphoton, time of flight three-dimensional radionuclide imaging. Med. Phys, **16**(5): 809-812.

Powell M.D., Monahan W.G. and Beattie W. (1970). Gamma-gamma coincidence detector. Radiology, 94: 197.

Rahmim A. and Zaidi H. (2008). PET versus SPECT: Strengths, limitations and challenges. Nucl. Med. Commun, **29**: 193–207.

Rangacharyulu C., Lai Thi Khanh Ly., Olshanoski K., Fukuchi T., Fukuda M., Kanda H. and Takahashi N. (2018). Gamma-ray Angular Correlations of Nuclear Beta Decays as a Novel Medical Imaging Modality. Annual Report of RCNP 2018; Available at https://www.rcnp.osaka-u.ac.jp/~annurep. Retrieved on March 18, 2021.

Rangacharyulu C., Lai Thi Khanh Ly., Olshanoski K., Santosh S., Nkuba L.L., Fukuchi T., Fukuda M., Kanda H., Msaki P.K., Sai K.V. and Takahashi N. (2020). Development of a Nuclear Gamma Cascade Correlations Based Medical Imaging System - A Novel Modality with Potentials for Replacement of SPECT and PET. International Conference on Clinical PET-CT and Molecular Imaging in the Era of Theranostics (IPET-2020). IAEA-CN-285/110.

Saffer J.R., Barrett H.H., Barber H.B. and Woolfenden J.M. (1992). Surgical probe design for a coincidence imaging system without a collimator. Image and Vision Comp, **10**(6): 333-341.

Santhosh R.S., Shyam D.S., Fukuchi T., Rangacharyulu C., Venkataramaniah K. and Sai K.V. (2019). Design and optimization of a collimator for a New PET system using GATE simulation. Proceedings, 64th DAE BRNS Symposium on Nuclear Physics : Lucknow (Uttar Pradesh), India. 2019; 852-853.

Schmitz-Feuerhake I. (1970). Studies on three-dimensional scintigraphy with gamma-gamma coincidence. Phys. Med. Biol**,** 15(4): 649-656.

Shimazoe K., Uenomachi M., Mizumachi Y., Takahashi H., Masao Y., Shoji Y., Kamada K., Yoshikawa A. (2017). Double Photon Emission Coincidence Imaging using GAGG-SiPM pixel detectors. JINST.12.C12055. 1-9. https://doi.org/10.1088/1748-0221/12/12/C12055.

Spyrou N.M., Mesbahi M.E. and Mallion S.N. (2000). Cascade gamma-gamma tomography and angular correlation measurements. Med. Imaging 2000 Phys. Med. Imaging, **3977**: 542–550.

Uenomachi M., Mizumachi Y., Yoshihara Y., Takahashi H., Shimazoe K., Yabu G., Yoneda H., Watanabe S., Takeda S., Orita T., Takahashi T., Moriyama F. and Sugawara H. (2018). Double Photon Emission Coincidence Imaging with GAGG-SiPM Compton Camera. Nuclear Instrum and Methods in Phys Research, A. 954(161682): 1-13. https://doi.org/10.1016/j.nima.2018.11.141

Uenomachi M., Shimazoe K., Ogane K. and Takahashi H. (2021a). Simultaneous multi-nuclide imaging via double-photon coincidence method with parallel hole collimators. Sci Rep, **11**(13330): 1-11. https://doi.org/10.1038/s41598-021-92583-4.

Uenomachi M., Takahashi M., Shimazoe K., Takahashi H., Kamada K., Orita T., Ogane K. and Tsuji A.B. (2021b). Simultaneous in vivo imaging with PET and SPECT tracers using a Compton-PET hybrid camera. Scientific Reports, **11**(17933): 1-11. https://doi.org/10.1038/s41598-021-97302-7.

von Boetticher H., Helmers H. and Muschol E.M. (1979). Contributions to depth discrimination γ-γ coincidence methods in scintigraphy. Phys. Med. Biol, **24**: 571–576.

von Boetticher H., Helmers H., Schreiber P. and Schmitz-Feuerhake I. (1982). Advances in γ-γ-coincidence scintigraphy with the scintillation camera. Phys. Med. Biol, **27**(12): 1495–1506.

Yoshihara Y., Shimazoe K., Mizumachi Y. and Takahashi H. (2017). Evaluation of double photon coincidence Compton imaging method with GEANT4 simulation. Nuclear Inst and Meth in Phy Res, A. **873**: 51–55.

Zacuto P., Rudin S. and Hart H.E. (1976). Performance characteristics of a focusing collimator coincidence scanning system. Phys Can (Special Issue), 32:14.1.